Nuclear Materials and Energy 30 (2022) 101133

Contents lists available at ScienceDirect

Nuclear Materials and Energy

journal homepage: www.elsevier.com/locate/nme

# Effect of neutron irradiation on ductility of tungsten foils developed for tungsten-copper laminates

Aleksandr Zinovev [a], Dmitry Terentyev [a], Chih-Cheng Chang [a,b], Chao Yin [a,b], Alexander Bakaev [a], Michael Rieth [c], Philipp Lied [c], Jens Reiser [c], Carsten Bonnekoh [c]

[a] Institute for Nuclear Materials Science, SCK CEN, Boeretang 200, 2400 Mol, Belgium
[b] Institute of Mechanics, Materials and Civil Engineering (iMMC), UCLouvain, Av. Georges Lemaître 4, 1348 Louvain-la-Neuve, Belgium
[c] Institute for Applied Materials, Karlsruhe Institute of Technology, 76344 Eggenstein-Leopoldshafen, Germany

ARTICLE INFO

*Keywords:*
Fusion
Advanced material
Divertor
DBTT
Embrittlement
DFT

ABSTRACT

Severe plastic deformation of tungsten (W) is known to be an efficient way to reduce its inherently high ductile-to-brittle transition temperature (DBTT), what is essential for its use in components of a fusion reactor. Thin rolled W foils possess superior mechanical behaviour at room temperature (RT), as demonstrated in previous works. It was then proposed to expand the beneficial mechanical properties of the foil to bulk by fabricating tungsten-copper (W-Cu) laminate composites, which can be used for structural applications. Neutron irradiation in HFIR resulted in embrittlement of the laminate already after 0.016 dpa, with the W foil determining the composite behaviour.

In this work, for the first time, we investigate the effect of neutron irradiation on individual W foil, and determine the resulting DBTT shift with the help of cantilever bend tests, using bulk W and the W-Cu composite as reference. The W foil and the bulk samples were irradiated to 0.15 dpa at 400 °C in the BR-2 reactor in Mol (Belgium). We also hypothesise that diffusion of Cu atoms into W could modify the response to irradiation in these materials. We substantiate it with complementary density functional theory (DFT) *ab initio* calculations to analyse the Cu-vacancy and Cu-self-interstitial interaction, which helps to elucidate co-alignment of the fluxes of point defects and Cu solutes in W matrix.

Irradiated foil was found to retain its ductility at RT. No significant irradiation hardening or DBTT shift were detected in the irradiated W foil compared to the bulk W. The different irradiation effect on embrittlement in individual foils and in the laminate may be attributed to the irradiation-assisted diffusion of Cu solutes in W foil, which could form intermetallic phases and affect the accumulation of lattice defects.

## Introduction

Tungsten (W), having the highest melting temperature among metals (3422 °C), high thermal conductivity (173 W/mK at RT) and other beneficial properties [1], is considered as a candidate material for future tokamak devices such as DEMO, stellarators, such as Advanced Reactor Innovation Evaluation Studies – Compact Stellarator (ARIES-CS) [2] and as a first wall material for inertial fusion devices [3,4]. For its application as a structural material, its inherently high ductile-to-brittle transition temperature (DBTT, which is in the range 25…500 °C, depending on purity, alloying elements and thermomechanical treatment [5]) has to be lowered, allowing for an expansion of the operation window of tungsten. Creation of an ultra-fine grained microstructure is considered one of the ways to ductilise tungsten [6].

This can be achieved by a cold rolling of a tungsten plate with the aim to obtain a thin foil. Foil sheets with thickness of 0.1 mm were fabricated by Plansee Metall GmbH (Austria) and investigated by Reiser et al. [7]. Severely rolled W foils exhibit superior material behaviour at RT (reduced DBTT compared to bulk W) due to the small grains, high amount of mobile edge dislocations, and the "foil effect" of dislocations annihilating on the surface [8,9]. In recent publications, necking in tensile test [10,11] and even stable crack propagation under quasi-static loads [12–14] or in fatigue experiments [15] have been reported. However, the ultrafine-grained microstructure of these foils is highly unstable already at 800 °C and grain coarsening is pronounced after a few minutes of annealing [16–18]. After a first initial drop in hardness, restoration decelerates and a relatively stable grain structure has formed with grain sizes around 1 μm [19].

High-temperature annealing could lead to recrystallization of fine-grain microstructure of W. Recrystallization and grain growth were observed in commercially-pure ITER-specification W fabricated by Plansee AG after annealing for 1 h above 1300 °C [20]. Annealing at

https://doi.org/10.1016/j.nme.2022.101133
Received 29 October 2021; Received in revised form 5 February 2022; Accepted 7 February 2022
Available online 10 February 2022

1100 °C was reported to cause recrystallization of the same pure W grade after 30…40 h. However, doping with 30 ppm of potassium (K) helped to delay the recrystallization until 200…300 h, while addition of 3 % of rhenium (Re) to pure and K-doped W suppressed recrystallization even during annealing for 3000 h at 1100 °C [21]. A similar effect is expected by applying a dispersion of $La_2O_3$ particles [22,23]. We refer the reader to the work of Palacios et al. [24] and consequent publications for further information about fabrication of foil from K-doped W and its mechanical properties.

To transfer the ductile properties of the foil to bulk, it was proposed to braze several layers of foil together with a Cu filler, forming a laminate composite [7]. Cu is a very ductile material and has high thermal conductivity (≈390 W/mK at RT) [25]. Charpy tests demonstrated high fracture toughness of the composite, highlighting it as a promising material to fabricate elements (like pipes, plates and blocks) for plasma facing components, including the DEMO divertor, to overcome a problem of neutron irradiation embrittlement during the nuclear phase operation [26]. Prototypes of three-dimensional components such as deep-drawn caps or pipes have already been fabricated from the W-Cu laminate and successfully tested under high heat flux [27].

Fission reactors are essential facilities for irradiation experiments on candidate materials for the fusion applications, and typically produce a flux of fast neutrons with the energy spectrum having a maximum around 2 MeV. The fission neutrons provide a convenient approximation of damage due to fusion neutrons, even though their energy does not match the mostly 14 MeV neutrons generated by the fusion reaction [28]. Various neutron irradiation campaigns have been carried out in several facilities, including JOYO and JMTR in Japan and the High Flux Isotope Reactor (HFIR) in the USA [29,30] to characterise tungsten for fusion applications.

A dedicated source of fast neutrons mimicking fusion spectrum would be the most appropriate testing facility to study the materials damage caused by a fusion reactor. At present, irradiation facilities providing the 14 MeV neutrons of fusion spectrum are scarce and do not pose sufficiently high flux and irradiation volume. An overview of qualification of materials in fission and fusion neutron spectra is given in [31]. The similarity in the initial defect cascade structures for fission and fusion irradiation conditions has been experimentally validated using a variety of low-intensity accelerator-based fast-neutron sources utilizing the deuterium–tritium reaction: including ASP in Aldermaston, UK; FNS at the Japanese Atomic Energy Agency (JAEA), Japan [32]; Technical University of Dresden, Germany; and the FNG at Frascati, Italy [33]. Other differences between fission and fusion neutron irradiations are expected to emerge at doses above ~ 10 dpa due to differences in transmutation [34] and are not relevant for the present study.

Facilities based on deuteron-stripping reaction, such as International Fusion Materials Irradiation Facility (IFMIF) [35,36] and IFMIF-DEMO Oriented NEutron Source (IFMIF-DONES) [37,38] would function by firing a beam of energetic deuterons at a lithium target to produce neutrons with a broad energy peak around 14 MeV, will provide higher dose rate and larger irradiation volume than the existing facilities, but are currently in the design/construction stage [28,39].

Another aspect affected by the neutron spectrum is the element transmutation in irradiated materials. The rate of transmutation of W to Re and Os in the fusion environment is expected to be lower than in the fission spectrum. Re and Os suppress the formation of voids and dislocation loops in W [40]. Thus more of those defects should be expected in W irradiated by the fusion neutrons than by fission neutrons, what affects the changes in mechanical properties. However, the rate of transmutation can be reduced down to values relevant to the fusion environment even when using a fission reactor, by shielding the specimens from thermal neutrons. Irradiation for the present paper has been carried out in a thick-walled stainless steel capsule placed inside a fuel element, what reduced the flux of thermal neutrons.

Garrison et al. [41] investigated the irradiation effects in W-Cu laminate composites for the first time with the help of tensile tests. The paper reports that after only 0.02 dpa irradiation at 410…450 °C the W foil in the laminate specimens started showing brittle fracture at RT. It is in contrast with expectations of a higher resistance to irradiation embrittlement, which should originate from the foil fine grain microstructure offering high density of sinks for mobile irradiation defects. Also, the irradiation embrittlement of W-CuCrZr laminate composite was reported recently in [42].

The observed irradiation embrittlement poses an important question whether the irradiation damage

1. has penalized ductile deformation of tungsten foils owing to the induced lattice defects,
2. or has enhanced/induced the diffusion between the joined sheets, leading to alternation of the irradiation defect accumulation, possible formation of intermetallic phases and, as an overall result, to a premature failure under mechanical load,
3. or, in synergy with elevated temperature, has caused a recovery of the cold-rolled beneficial microstructure.

To single out the influence of the Cu-W joint between the laminate components on the irradiation embrittlement of the composite, specimens made of the W foil and a reference bulk W were irradiated in the same capsule up to 0.15 dpa at 400 °C, in the low temperature range as studied earlier by Garrison et al. [41]. The impact of the neutron irradiation on the DBTT shift in foils and bulk samples was analysed by means of mechanical tests. To understand the impact of the thermally-induced recovery of the foil microstructure on the irradiation-induced embrittlement, two sets of foil specimens were irradiated and tested in equivalent conditions: (i) as-rolled and (ii) annealed at 800 °C for 1 h.

Another factor possibly affecting the ductility of W foil in the composite might be the diffusion of Cu atoms from the W-Cu interfaces across the W layers. The possibility of such diffusion process was shown with the help of X-ray diffraction (XRD) tests [43] and molecular dynamics simulations [44]. A W-Cu joint produced by applying an external pressure of 106 MPa at 980 °C for 180 min was analysed in an atomic-scale resolution scanning transmission electron microscope, where mutual diffusion of Cu and W was confirmed, with the flux of Cu atoms into W being dominant [44].

Certainly, the irradiation temperature of the composites studied in [41,42] was much lower than the temperature of fabrication of the composite in [44], however irradiation could accelerate/induce the diffusion/permeation of Cu atoms into W layers owing to an increased concentration of point defects caused by the collisions with neutrons. Note that the irradiation at 400 °C already implies a long-range vacancy diffusion in tungsten [45]. The diffusion of Cu atoms inside W foils could affect the accumulation of the irradiation damage in W (by trapping of irradiation defects), and could lead to the formation of non-equilibrium phases such as CuW3 and Cu3W [44]. In both situations, plastic deformation should be suppressed.

As a matter of fact, the radiation-induced segregation (RIS) is known to have a strong impact on the phase stability, embrittlement and other physical–chemical phenomena occurring under irradiation. In particular, the segregation of Cr on both ⟨1 0 0⟩ and ½⟨1 1 1⟩ dislocation loops is a well-established phenomenon, which has been reported for different grades of Fe–Cr steels and model alloys [46–48], as well as in austenitic steels [49]. Irradiated-induced precipitation of the χ phase in tungsten-rhenium alloys was reported as well [50–52].

To substantiate the discussion and elucidate the mechanism of Cu-defect migration in W, we have performed DFT calculations to assess the interaction of Cu atoms in W bulk with a vacancy and self-interstitial atom.

## Materials and methods

### Tungsten foil

The studied W foil is part of a set of severely deformed W materials, which were produced applying an industrial powder metallurgy (PM) route. Rolling of the foil included hot deformation of the sintered compact, subsequent warm rolling to a logarithmic strain of 3.7, and finally, 0.4 conducted by cold rolling, which resulted in a total persistent strain of 4.1. Warm and cold rolling was carried out in a strictly unidirectional manner. Detailed information on the production process and resulting microstructural modifications are given in an earlier publication [53].

Specimens of the W foil were cut out by electrical discharge machining (EDM), after which half of them were heat treated at 800 °C (30 % of the melting temperature) for 1 h using a tube furnace. After pumping the air from the tube, the furnace was heated up. Shortly after the furnace thermocouples indicated reaching the target temperature, the specimens were inserted into the heating zone by a slider. The 1 h count down started after the difference between the actual temperature of the specimen (measured by a thermocouple in the slider located below the crucible) and the target temperature was <20 °C. After the targeted duration of 1 h was reached, the crucible was retracted from the furnace and cooled down under vacuum.

### Bulk IGP tungsten

Commercially-pure W rod with a square 36 mm × 36 mm cross section was supplied by Plansee AG (Austria). The material was fabricated by powder metallurgy, the final bar was hammered on both sides, what resulted in carrot-shaped grains, and underwent a stress relief heat treatment. The final product satisfies the ITER specification [54], and we refer to this material as “IGP”, standing for “ITER Grade Plansee”. The details and thermo-mechanical properties of this material before and after irradiation were described in open literature [55–59].

### Neutron irradiation in BR-2

Neutron irradiation of tensile specimen of pure IGP W and the W foil specimens was carried out in the fission Belgian Reactor 2 (BR2) of SCK CEN. Two stacks of as-rolled and annealed foil specimens, 29 in each, were irradiated together with five tensile specimens of IGP W in a stainless steel capsule filled with an inert gas (helium) to prevent oxidation during the irradiation. The specimens inside the capsule were secured and centred by a special holder in order to maintain a specific gap between the stack of specimens and the capsule wall to achieve the required irradiation temperature. The capsule was positioned in an irradiation rig, introduced inside a fuel element of BR2 to maximize the ratio of fast to thermal neutrons.

The thick walls of the stainless steel capsule (1.5 mm) shielded the specimens from thermal neutrons, significantly suppressing transmutation in the investigated materials. As a result, the rate of transmutation of W into rhenium (Re) and then into osmium (Os) was 1.87 at. % Re/dpa and 0.192 at.% Os/dpa, as calculated by MCNP6. Note that the transmutation rate in the laminates irradiated in HFIR and reported by Garrison et al. [41] was higher, reaching 5 % Re/dpa and 0.5 % Os/dpa [41,60]. MCNP is a general-purpose Monte Carlo N-Particle code that can be used for neutron, photon, electron, or coupled neutron/photon/electron transport [61].

The specimens were irradiated for 36 days at 400 °C, exposed to an average flux of fast neutrons $7.1 \times 10^{13}$ n/cm$^2$/sec (E > 1 MeV). The irradiation resulted in the fluence of $2.21 \times 10^{20}$ n/cm$^2$ (E > 1 MeV), equivalent to displacement damage around 0.15 dpa. The neutronics calculation was performed with the help of MCNP6 using a threshold displacement energy ($E_d$) of 55 eV [62].

### Tensile tests

Small dog-bone shaped specimens, as are shown in Fig. 1a, were used for uniaxial tensile tests of IGP W. The total length of the specimens was 16 mm with a gauge length of 5.2 mm and an effective cross section of 2.4 mm$^2$ (1.6 mm × 1.5 mm, irradiated and some non-irradiated specimens) or 2.88 mm$^2$ (1.6 mm × 1.8 mm, non-irradiated specimens). The choice of the miniaturised specimen geometry is substantiated in the work of Yin et al. [63] along with a review of factors ensuring that the obtained mechanical properties are not affected by the specimen dimensions. Tensile tests of non-irradiated samples of IGP W are reported in that paper as well.

The tests on irradiated specimens were conducted in air, in a hot cell of SCK CEN on an Instron 8501 universal mechanical testing machine, equipped with a 100 kN load cell. The values of load and the crosshead displacement were recorded during the test, after which they were used to calculate engineering stress and strain in the specimen. Given the need to work with miniaturised specimens in a hot cell with mechanical manipulators, the use of extensometers for strain measurement was considered impractical. In the same time, Motra et al. [64] showed that strain calculated from the crosshead displacement is comparable to that measured directly, and the need to use an extensometer emerges when the elastic modulus has to be estimated from tensile tests. In order to reduce the displacement uncertainty, the test bench was calibrated and qualified according to the industrial ASTM standard before performing the tests. With the elongation of tensile specimens at fracture expected to be in the range of several hundred μm to a few mm (depending on temperature), and with the resolution of the LVDT (linear variable differential transformer) which measures the crosshead displacement being around several μm, we consider that it returns strain with adequate precision for the present research.

A special holder was designed, shown in Fig. 1b (without removable covers, to expose the mounted specimen). To align the specimens in the testing machine, they were preloaded to 100 N before heating. The tests were performed at a constant displacement rate of 0.2 mm/min, corresponding to the strain rate of $6.4 \times 10^{-4}$ 1/s.

### Cantilever bending tests of foils

Both, as-rolled and annealed foils were cut into specimens 16 × 4.2 mm$^2$ identical to the tensile specimen dimensions (Fig. 2b). A special setup was designed (shown in Fig. 2a) and fabricated from Nimonic 90 alloy to perform bend tests on an Instron machine in the cold lab, as well as in the hot cell. One half of the foil specimen (2) is clamped in the holder (1) by the cover (3) which is secured by two M5 × 16 screws (5). The assembly is fixed in the testing machine on the lower pulling/pushing rod, while the upper rod is equipped with the stamp (4), which exerts force on the other half of the foil specimen.

The speed of the lower crosshead was set to be 0.72 mm/min during the tests to maintain a quasi-static deformation behaviour, performed in a temperature range −100…25 °C, with liquid nitrogen as coolant. In contrast with the tensile tests, no preloading was applied to the foil specimens. The values of load and deflection were recorded during the test. A photo of the bent specimen in the setup is shown in Fig. 2c (the corresponding area is encircled in Fig. 2a), where the specimen has not fractured, even though the stamp has reached its lowest position. The camera had shallow depth of field, and was focused on the foil specimen; that is why the stamp and the holder are blurred. The specimens could be bent up to the deflection angle of 60° at the lowest position of the stamp. If a specimen did not fracture up to that point, it was considered ductile. After dismounting, the deflection angle of ductile specimens usually reduced to 30…45° due to elastic unloading.

### DFT calculations

Density functional theory (DFT) calculations were done with the

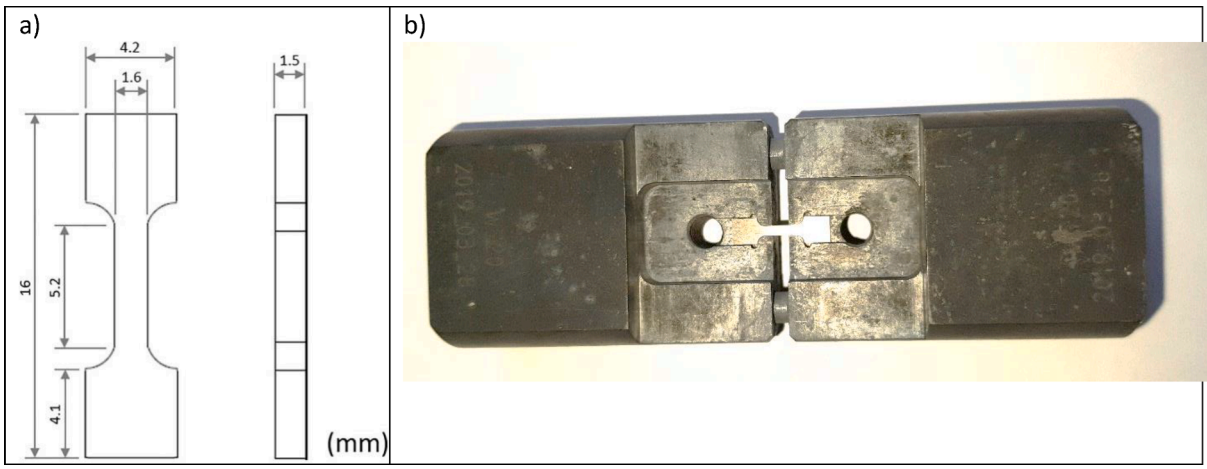


**Fig. 1.** a) The drawing of the tensile specimen used to characterise IGP W (non-irradiated specimens with thickness 1.8 mm were also used). b) A specimen mounted in a special holder for tensile tests (without removable covers).

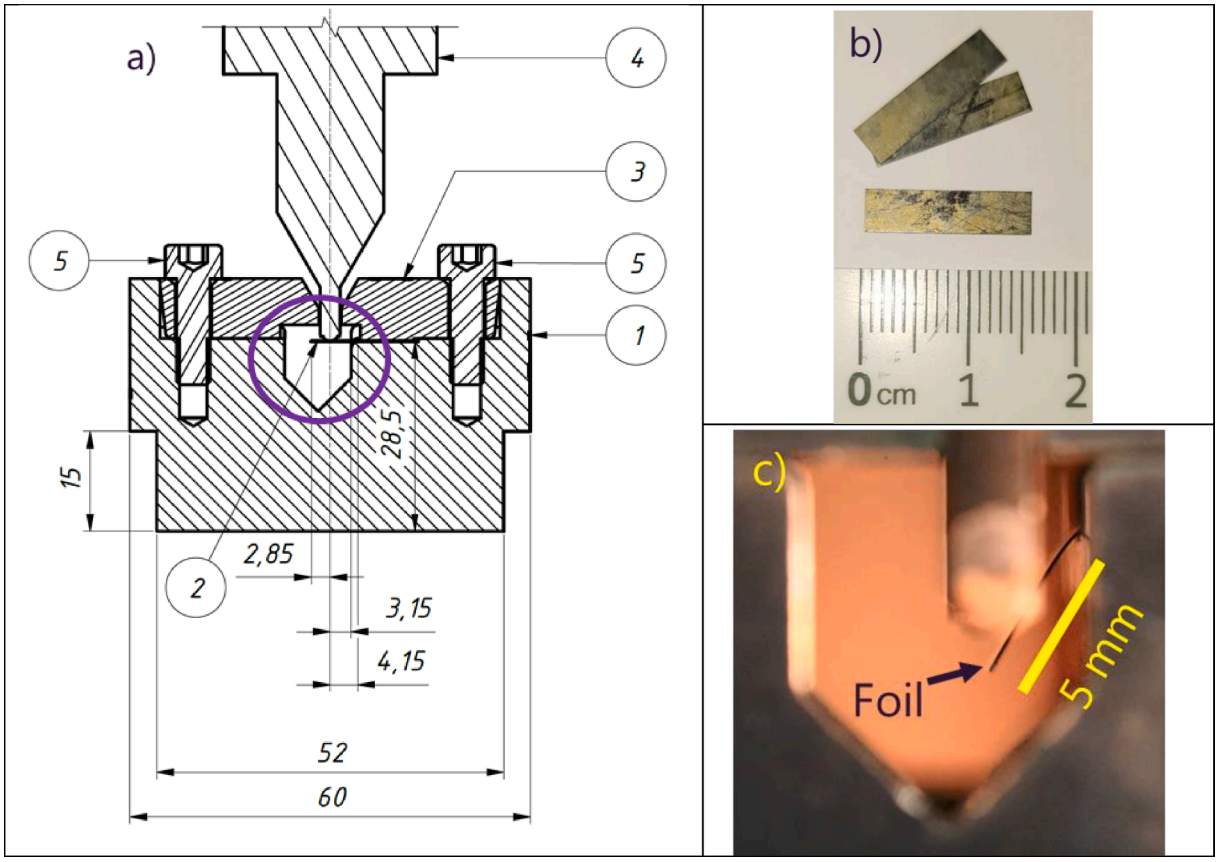


**Fig. 2.** a) Drawing of the setup for cantilever bend tests of foil specimens. b) The foil specimens 16 × 4.2 mm$^2$. c) A photograph of the foil specimen bent to the maximum deflection angle of 60°.

Vienna Ab initio Simulation package (VASP) [65,66] using the projector-augmented wave (PAW) pseudopotentials [67,68]. The generalized gradient approximation with the parameter set by Perdew, Burke and Ernzerhof (PBE) [69] was applied to account for the exchange–correlation effects. The analysed atomic configurations were non spin-polarized (i.e. non-magnetic). The pseudopotentials with six valence electrons for W and 11 for Cu were utilized. Ionic relaxation was performed by means of the conjugate gradient algorithm with a force convergence criterion of 0.03 eV/Å. The relaxation of the electronic subsystem was realized with a global break condition of $10^{-4}$ eV. A Methfessel-Paxton smearing of 0.3 eV has been applied.

The simulation box had the dimensions of 5 × 5 × 5 with the lattice constant $a_0$ = 3.178 Å. The k-point mesh of 5 × 5 × 5 and the cut-off energy equal to 450 eV were applied following the previous study [70]. Only structural relaxation was allowed during the energy minimization procedure.

The migration barrier for the exchange of a Cu-vacancy pair was calculated using the nudged elastic band (NEB) method with seven intermediate images.

The interaction energy between the defects 1 (Cu impurity) and 2

(whether a vacancy or a self-interstitial atom, SIA, with orientation ⟨110⟩, ⟨111⟩ or ⟨221⟩ ) was calculated following [71]:

$$E_i = E_{defects1-2} + E_{pure} - \left(E_{defect1} + E_{defect2}\right)$$

where $E_{pure}$ is the total energy of a defect-free crystal, $E_{defects1-2}$ is the total energy of a crystal containing both defects 1 and 2, while $E_{defect1}$ and $E_{defect2}$ denote the total energy of a crystal with an isolated defect 1 or defect 2, respectively. Following this notation, a negative interaction energy implies an attractive interaction, and vice versa.

## Results

### *Tungsten foil*

Visual inspection of the tested specimens, whose examples are shown in Fig. 3, helped to identify whether they experienced brittle fracture or ductile bending. The arrows with letters "L", "T" and "N" denote the rolling direction (which is the same in all the steps of warm and cold rolling of the foil material), the transverse direction (in-plane) and the normal direction of the foil specimens, respectively. The presence of cracks on the folds of specimens indicated brittle fracture, as shown in Fig. 3a. A smooth, crack-free fold and elastic unloading back to the angle 30…45° were typical features of ductile bending, as shown in panels (c) and (d) of Fig. 3, correspondingly. As a rule, several specimens were tested at each temperature (up to four in the transition region) to reveal the typical deformation modes.

As expected, with the increase of test temperature, the specimens were more likely to experience ductile bending rather than brittle fracture. Fig. 4 summarises the fraction of the ductile specimens per test temperature. The fraction ranges from zero at low temperature to a unity at high temperature. Thus, we chose to define the transition temperature at the fraction of brittle specimens equal to 0.5, i.e., where 50 % of tested specimens fracture in the brittle way. Since the tests were carried out at discrete values of temperature, we assume that the transition temperature can be defined with the precision of 25 °C (i.e., ±12.5 °C), which is adequate for the initial assessment of embrittlement.

The results show that the as-rolled foil had the lowest DBTT before the irradiation (between −100 °C and −75 °C). The DBTT has increased by 25…50 °C after the irradiation. The non-irradiated annealed foil had DBTT between −50 °C and −25 °C, which did not change significantly after the irradiation. Irradiated annealed specimens were all ductile at −25 °C, but one specimen experienced brittle fracture at 0 °C. Thus the pre-irradiation annealing at 800 °C for 1 h did not affect significantly the consequent shift of DBTT due to the irradiation.

Examples of the load–deflection curves of the foil specimens obtained in the DBTT region are grouped in Fig. 5 by grade and irradiation. Data for the annealed foil specimens are represented on top, while for the as-rolled ones are in the bottom. Left and right columns correspond to non-irradiated and irradiated specimens. Brittle specimens demonstrate sudden drop of applied load at low deflection, when they fracture. Ductile specimens sustain deflection up to ≈3.2 mm (about 60° deflection angle) without fracture. Irregularities on the curves can be attributed to the friction between the stamp and the specimen, which increased with the deflection angle, as well as due to the formation of ice on the specimens during the tests carried out at negative temperature. However, video registration could unambiguously discern the deformation mode (brittle or ductile).

The maximum load measured in bend tests of the foil specimens is summarised in Fig. 6, for as-rolled (left) and annealed (right) foils. The spurious peaks visible on the curves on Fig. 5 were disregarded and substituted with an average value of the load measured before and after the peak. The symbol shape corresponds to deformation mode (brittle/ductile) while the fill colour indicates the irradiation state. This plot also helps to visualise the DBTT region for each foil state. The irradiation hardening estimated in this way in the ductile region amounts to 1…2 N (10…30 %) for both as-rolled and annealed foils (with the dashed lines highlighting the trends). Note that the single annealed irradiated specimen which showed the brittle fracture at 0 °C appears to be an outlier from the trend (encircled), and should not be taken into consideration for the estimation of DBTT.

### *Bulk IGP tungsten*

The DBTT shift of the bulk IGP tungsten specimens, which were irradiated together with the foils, was assessed with the help of tensile tests. The stress–strain curves of non-irradiated and irradiated specimens are presented in Fig. 7a (the curves of irradiated specimens are offset by 6 % of engineering strain for easier comparison). Tensile tests revealed significant hardening (around 70 % at 400…500 °C), early necking (loss of uniform elongation) and reduction of total elongation (by the factor of ≈2.5 at 400…500 °C), as a consequence of the irradiation. Given the lack of tensile specimens of the bulk material (and the laminate composite specimens described in Discussion), we could not repeat the assessment of transition temperature based on the fraction of brittle specimens (what has been done for the foil specimens), and can only report the range of temperature separating a single brittle fracture from a single ductile response of the material, before and after irradiation. On top of that, since different mechanical tests were used to evaluate the transition temperature, care should be exercised when comparing their values obtained for W foil and bulk. However, the shift of transition temperature should be less dependent on the applied method and could be used to assess the effect of irradiation under the

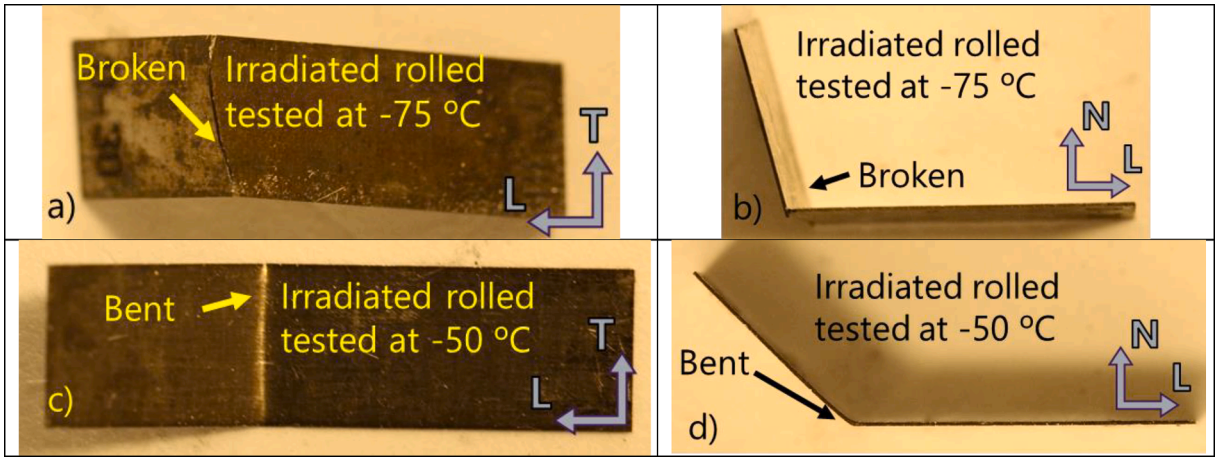


**Fig. 3.** Photographs of bent foil specimens irradiated to 0.15 dpa at 400 °C, revealing brittle fracture (a, b) or ductile bending (c, d).

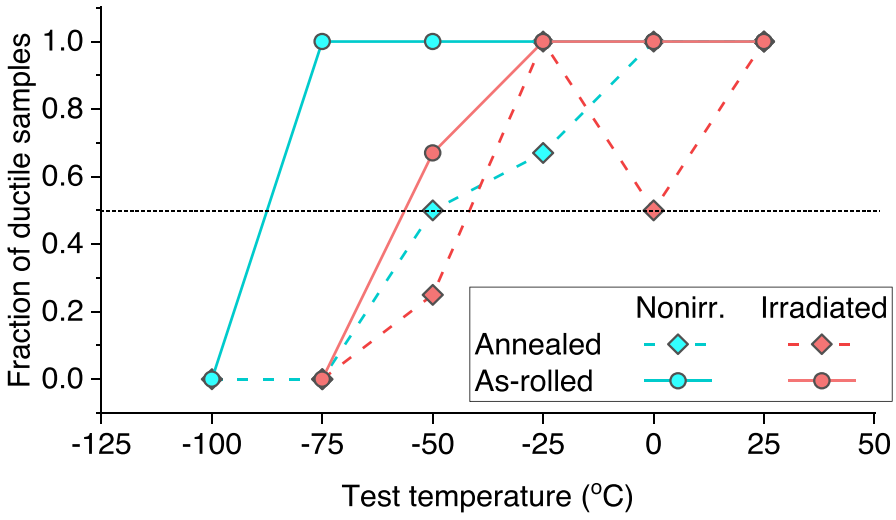


**Fig. 4.** Fraction of ductile foil specimens at a given temperature, before and after irradiation to 0.15 dpa at 400 °C.

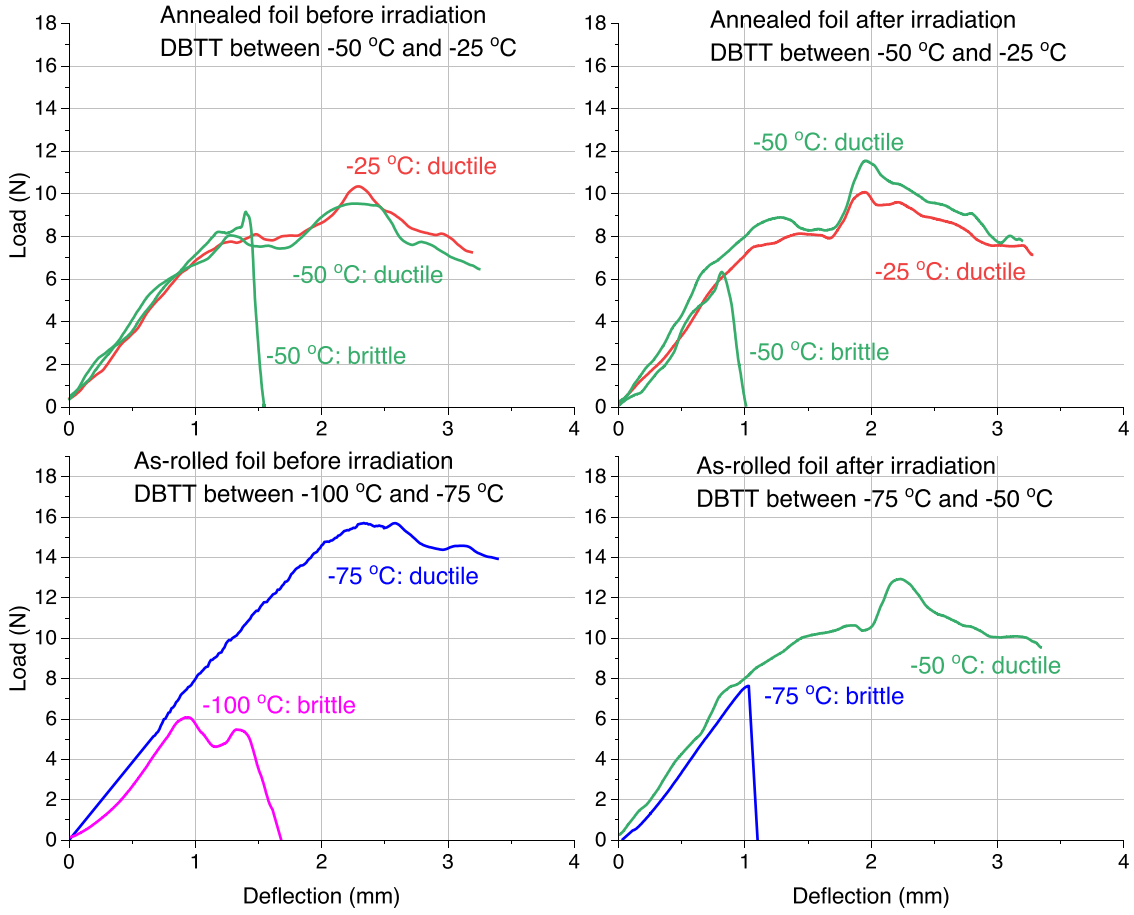


**Fig. 5.** Examples of load–deflection curves of foil specimens obtained in bend tests before and after the irradiation to 0.15 dpa at 400 °C.

same conditions on the two materials. The irradiated material was ductile at 400 °C and brittle at 375 °C, while the non-irradiated material was ductile at 200 °C and brittle at 150 °C. Thus, the shift of DBTT of bulk tungsten irradiated at 400 °C up to 0.15 dpa is 200…250 °C. Clearly, the shift of DBTT and increase of the ultimate tensile strength is much larger in the bulk samples as compared to the foil specimens.

## Discussion

The fact that the foil specimens irradiated to 0.15 dpa demonstrated much smaller DBTT shift than the bulk tungsten could be attributed to (i) a high density of structural defects (i.e. grain boundaries, dislocation debris) in the foil, which should serve as sinks for mobile irradiation-induced defects, and (ii) to the "foil effect" of dislocations annihilating on the foil surface during bending [9,41]. Since the foil in both states is

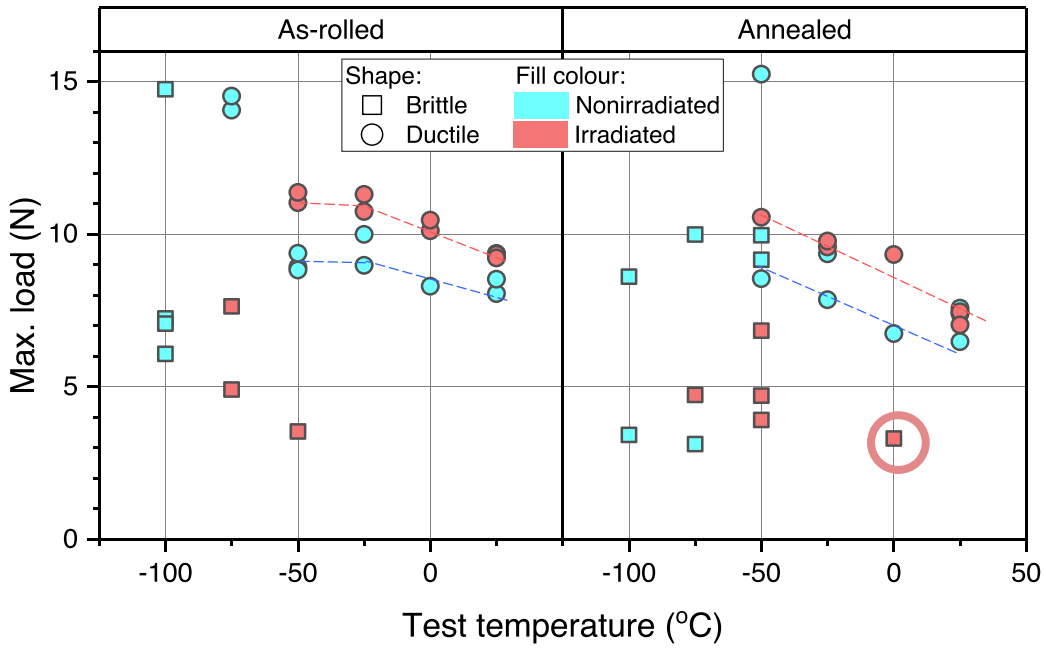


**Fig. 6.** Maximal load measured in bend tests of foil specimens as a function of test temperature.

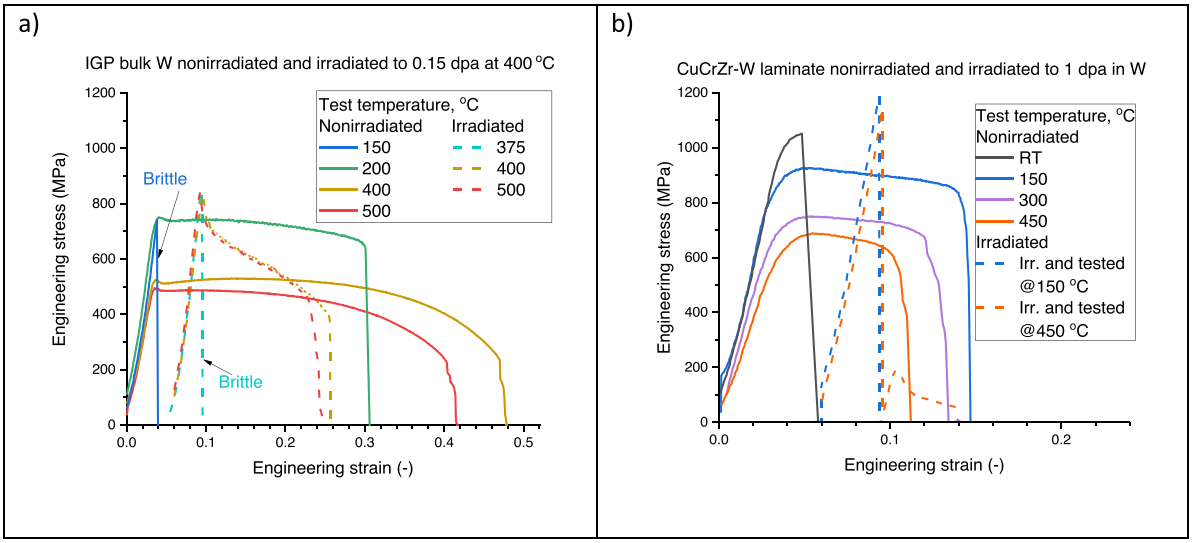


**Fig. 7.** Stress–strain curves of (a) bulk IGP tungsten before and after irradiation to 0.15 dpa at 400 °C, (b) W-CuCrZr laminate composite before and after irradiation to 1 dpa at 150 °C or 450 °C.

found to remain essentially ductile after the irradiation, one should address the effect of neutron irradiation on the joint between CuCrZr and W layers in order to explain the irradiation embrittlement found in the composites.

*W-CuCrZr laminate composite*

The effect of the neutron irradiation on individual foil specimens and on a tungsten laminate composite could be compared. The laminate consists of repeated layers of tungsten foil and a CuCrZr interlayer (0.1 mm each), joined together into a multilayer material. More information about the production can be found in [26,27] and the post-irradiation mechanical properties of this material can be found in our recent paper [42]. Tensile specimens were produced from the laminate using the same drawing as for IGP W (Fig. 1) but with a thickness of 1 mm, in such a way so that the uniaxial tensile load would be applied parallel to the interface between the laminate constituents. A number of specimens were irradiated by neutrons in the BR2 reactor at 150 °C, 350 °C and 450 °C to 1 dpa in W, which is a higher dose than that in the individual foil specimens. Then they were mechanically tested in a hot cell at SCK CEN at 150 °C and at their irradiation temperature and crosshead speed of 0.2 mm/min ($6.4 \times 10^{-4}$ 1/s).

Fig. 7b summarises the engineering stress–strain curves of the laminate specimens (the curves of irradiated specimens are offset by 6 % of engineering strain for easier comparison). The tests confirmed that the non-irradiated laminate is ductile between 150 °C and 450 °C. However, the irradiation has eliminated its ductility and caused hardening up to 70 % (at 450 °C). Note that the strength of the laminate is higher than that of bulk W in both irradiated and non-irradiated states.

Fig. 8 presents SEM images of the fracture surface of the irradiated laminate specimen irradiated and tested at 350 °C. Fig. 8a shows a zoomed region of the laminate with a W foil stacked between two layers

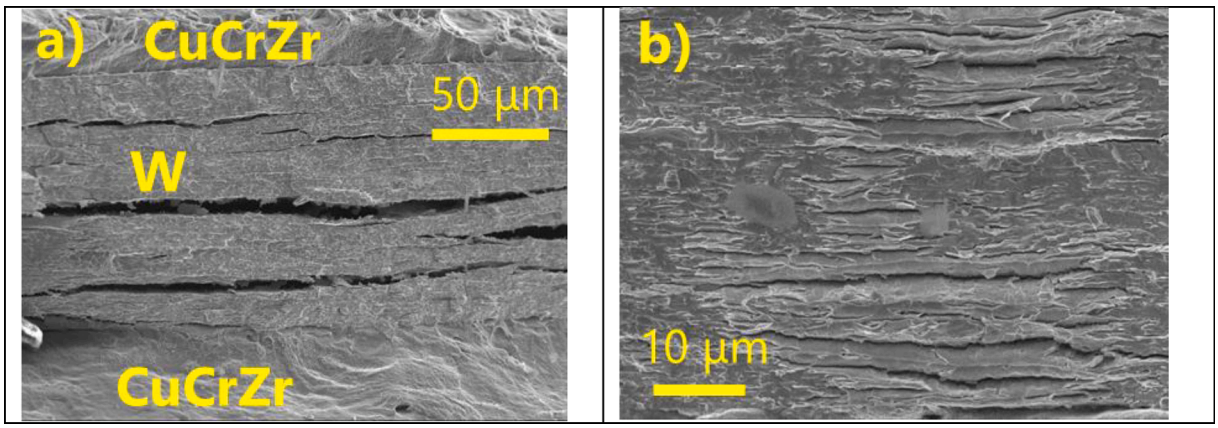


**Fig. 8.** Fracture surface of a laminate specimen irradiated and tested at 350 °C. a) Showing a W foil stacked between two CuCrZr layers. b) Highlighting a number of "knife edges" (plastically deformed grains) in the W foil.

of CuCrZr. A good bonding between the composite constituents was regularly observed, in which case longitudinal cracks usually formed within the tungsten foil. It could indicate the generation of the out-of-plane tensile stress component (normal to the foil surface) acting on the W foils during uniaxial tensile tests. In this case, the brittle fracture of W foil in the composite may be explained not only by a larger irradiation damage dose than in the individual foil specimens, but also by a different stress state (what could also be the case in the composite samples irradiated to a lower dose in [41]). The CuCrZr layers exhibited purely ductile deformation with characteristic dimples. Fig. 8b shows a close-up view of the W foil in which most of the grains experienced transgranular brittle cleavage. However, some grains deformed more readily, even forming so-called "knife edges", which shows that plasticity is not completely suppressed in the tungsten foil in the composite.

*DFT calculations*

The results of the DFT calculations have shown that the Cu-vacancy interaction energy in the 1st, 2nd and 3rd nearest neighbour (1nn, 2nn and 3nn) amounts to −0.16 eV, 0.24 eV and 0.09 eV, respectively. In addition, the migration barrier for the vacancy-solute 1nn exchange is significantly lower for Cu (0.43 eV) than the migration of a vacancy in bulk W (1.68 eV). The identified attractive interaction of 1nn vacancy-solute pairs together with a repulsive interaction of 2nn vacancy-solute pairs indicate the absence of a vacancy-solute drag, and imply the opposite direction of fluxes of vacancies and Cu solutes in W.

The SIA defects are known to be highly mobile in W with the migration energy of just 0.003 eV [40]. A Cu atom forms a stable complex with SIA defects (mixed interstitial configuration oriented along the ⟨1 1 1⟩ direction) with the interaction energy of −3.44 eV. The difference between the total energies of the mixed interstitials with Cu of orientations ⟨1 1 0⟩ and ⟨1 1 1⟩ is equal to −0.08 eV, i.e., nearly athermal. It means that the on-site rotations of the mixed interstitial configurations with Cu are possible in W.

Therefore, a strong binding of Cu with ⟨1 1 1⟩ crowdions and capability to perform on-site rotation may lead to the drag of Cu solutes by SIA in W. In turn, the presence of Cu solutes in W will strongly hinder the 1-D migration of SIA clusters, promoting the nucleation of dislocation loops, which will contribute to the irradiation hardening.

Thus, the performed complementary DFT calculations point out that the influx of the Cu solutes (moving opposite to the flux of vacancies) from the W-Cu interface is possible given the binding energy landscape for the vacancy-Cu interaction and reduced migration energy barrier. Subsequently, the effect of Cu on the accumulation of the irradiation-induced lattice defects and potential formation of the W-Cu intermetallic phases may occur. Experimental clarification of the microstructure is needed to reconfirm the hypothesis above.

## Conclusions

In this work we have assessed the impact of neutron irradiation on ductility of tungsten foils developed for the application in W-Cu laminates. The as-rolled and 800 °C-annealed foils were irradiated up to 0.15 dpa at 400 °C. To reveal the specific effects in the foils, a number of bulk tungsten specimens were also irradiated in equivalent conditions. The DBTT shift in the foils was estimated on the basis of bend tests and by video registration and is found to be:

- <50 °C for the as-rolled foil, with DBTT increasing from −100…−75 °C to −75…−50 °C due to the irradiation,
- <25 °C for the annealed foil, with DBTT remaining in the range −50…−25 °C before and after the irradiation.

At the same time, the DBTT shift in the irradiated bulk W specimens was found to be in the range 200…250 °C, which is much higher than the one found for foils. This result demonstrates that the fine microstructure of the foils (even after extended recovery during annealing at 800 °C) is indeed beneficial for the resistance against irradiation damage.

Annealing at 800 °C for 1 h did increase the DBTT of non-irradiated foil by ≈50 °C, but has not led to a significant DBTT shift in the irradiated material, as compared to the as-rolled foil. Irradiation hardening in the foil in both as-rolled and annealed states was found to be much lower (max. load increased by 10…30 %) compared to the bulk tungsten, which demonstrated hardening up to 70 %.

Correspondingly, the individual foil specimens showed ductile behaviour at temperatures much lower than the foil in the W-CuCrZr laminate. Therefore, the irradiation embrittlement of the W-Cu laminate composite might originate from the irradiation-induced diffusion of Cu (or other chemical elements present at the W-Cu interface) into the tungsten foil. A complementary DFT calculation indicated that the fluxes of Cu solutes and vacancies in W would be directed opposite to each other, and that self-interstitial atoms in W are able to drag Cu solutes, suggesting that an influx of Cu atoms into W layers from the W-Cu interfaces may indeed occur. The presence of Cu solutes in W may affect the accumulation of irradiation-induced lattice defects in W and lead to formation of intermetallic phases.

In conclusion, the present study points to a better resistance of the tungsten foil (in both as-rolled and annealed states) to irradiation up to 0.15 dpa at 400 °C as compared to bulk tungsten. The limits for the resistance of the foils against irradiation damage (in terms of irradiation dose and temperature) should be further explored. The origin of the embrittlement of laminate composite materials based on W foil should be addressed after irradiation of foil and laminate to similar doses at identical temperatures.

*CRediT authorship contribution statement*

**Aleksandr Zinovev:** Investigation, Validation, Visualization, Writing – original draft, Writing – review & editing. **Dmitry Terentyev:** Conceptualization, Writing – original draft, Writing – review & editing, Supervision, Project administration, Funding acquisition. **Chih-Cheng Chang:** Investigation. **Chao Yin:** Investigation, Visualization. **Alexander Bakaev:** Methodology, Software, Investigation, Writing – original draft. **Michael Rieth:** Conceptualization, Writing – original draft, Supervision, Project administration. **Philipp Lied:** Resources, Writing – original draft. **Jens Reiser:** Conceptualization, Methodology, Resources. **Carsten Bonnekoh:** Resources, Writing – original draft.

## Declaration of Competing Interest

The authors declare that they have no known competing financial interests or personal relationships that could have appeared to influence the work reported in this paper.

## Acknowledgements

This work has been carried out within the framework of the EUROfusion Consortium and has received funding from the Euratom research and training programme 2014-2018 and 2019-2020 under grant agreement No 633053. The views and opinions expressed herein do not necessarily reflect those of the ITER Organization or of the European Commission. We acknowledge the CINECA award under the ISCRA initiative, for the availability of high performance computing resources and support.

## References

[1] M. Li, M. Sommerer, E. Werner, S. Lampenscherf, T. Steinkopff, P. Wolfrum, J.-H. You, Experimental and computational study of damage behavior of tungsten under high energy electron beam irradiation, Eng. Fract. Mech. 135 (2015) 64–80, https://doi.org/10.1016/j.engfracmech.2015.01.017.

[2] T.K. Mau, T.B. Kaiser, A.A. Grossman, A.R. Raffray, X.R. Wang, J.F. Lyon, R. Maingi, L.P. Ku, M.C. Zarnstorff, Divertor Configuration and Heat Load Studies for the ARIES-CS Fusion Power Plant, Fusion Sci. Technol. 54 (2008) 771–786. 10.13182/FST08-27.

[3] G. Pintsuk, A. Hasegawa, Tungsten as a Plasma-Facing Material, in: Compr. Nucl. Mater., 2nd ed., Elsevier, 2020: pp. 19–53. 10.1016/B978-0-12-803581-8.11696-0.

[4] F. Najmabadi, A.R. Raffray, S.I. Abdel-Khalik, L. Bromberg, L.A. El-Guebaly, D. Goodin, D. Haynes, J. Latkowski, W. Meier, R. Moore, S. Neff, C.L. Olson, J. Perkins, D. Petti, R. Petzoldt, D. V. Rose, W.M. Sharp, P. Sharpe, M.S. Tillack, L. Waganer, D.R. Welch, M. Yoda, S.S. Yu, M. Zaghloul, Operational Windows for Dry-Wall and Wetted-Wall IFE Chambers, Fusion Sci. Technol. 46 (2004) 401–416. 10.13182/FST04-A580.

[5] J.W. Davis, V.R. Barabash, S.A. Fabritsiev, 2.2 Tungsten, in: Mater. Assess. Report. ITER Handb. (G 74 MA 10), n.d.

[6] M. Faleschini, H. Kreuzer, D. Kiener, R. Pippan, Fracture toughness investigations of tungsten alloys and SPD tungsten alloys, J. Nucl. Mater. 367–370 A (2007) 800–805, https://doi.org/10.1016/j.jnucmat.2007.03.079.

[7] J. Reiser, M. Rieth, B. Dafferner, A. Hoffmann, Tungsten foil laminate for structural divertor applications – Basics and outlook, J. Nucl. Mater. 423 (1-3) (2012) 1–8, https://doi.org/10.1016/j.jnucmat.2012.01.010.

[8] J. Reiser, M. Rieth, B. Dafferner, A. Hoffmann, X. Yi, D.E.J. Armstrong, Tungsten foil laminate for structural divertor applications – Analyses and characterisation of tungsten foil, J. Nucl. Mater. 424 (1-3) (2012) 197–203, https://doi.org/10.1016/j.jnucmat.2012.02.030.

[9] J. Reiser, M. Rieth, A. Möslang, B. Dafferner, A. Hoffmann, X. Yi, D.E.J. Armstrong, Tungsten foil laminate for structural divertor applications – Tensile test properties of tungsten foil, J. Nucl. Mater. 434 (1-3) (2013) 357–366, https://doi.org/10.1016/j.jnucmat.2012.12.003.

[10] S. Bonk, J. Hoffmann, A. Hoffmann, J. Reiser, Cold rolled tungsten (W) plates and foils: Evolution of the tensile properties and their indication towards deformation mechanisms, Int. J. Refract. Met. Hard Mater. 70 (2018) 124–133, https://doi.org/10.1016/j.ijrmhm.2017.09.007.

[11] P. Lied, W. Pantleon, C. Bonnekoh, S. Bonk, A. Hoffmann, J. Reiser, M. Rieth, Comparison of K-doped and pure cold-rolled tungsten sheets: Tensile properties and brittle-to-ductile transition temperatures, J. Nucl. Mater. 544 (2021) 152664, https://doi.org/10.1016/j.jnucmat.2020.152664.

[12] C. Bonnekoh, A. Hoffmann, J. Reiser, The brittle-to-ductile transition in cold rolled tungsten: On the decrease of the brittle-to-ductile transition by 600 K to − 65 °C, Int. J. Refract. Met. Hard Mater. 71 (2018) 181–189, https://doi.org/10.1016/j.ijrmhm.2017.11.017.

[13] V. Nikolić, S. Wurster, D. Firneis, R. Pippan, Fracture toughness evaluation of UFG tungsten foil, Int. J. Refract. Met. Hard Mater. 76 (2018) 214–225, https://doi.org/10.1016/j.ijrmhm.2018.06.008.

[14] J. Reiser, S. Wurster, J. Hoffmann, S. Bonk, C. Bonnekoh, D. Kiener, R. Pippan, A. Hoffmann, M. Rieth, Ductilisation of tungsten (W) through cold-rolling: R-curve behaviour, Int. J. Refract. Met. Hard Mater. 58 (2016) 22–33, https://doi.org/10.1016/j.ijrmhm.2016.03.006.

[15] S. Pillmeier, S. Žák, R. Pippan, A. Hohenwarter, Influence of cold rolling on the fatigue crack growth behavior of tungsten, Mater. Sci. Eng. A. 805 (2021) 140791, https://doi.org/10.1016/j.msea.2021.140791.

[16] V. Nikolić, S. Wurster, D. Firneis, R. Pippan, Improved fracture behavior and microstructural characterization of thin tungsten foils, Nucl. Mater. Energy. 9 (2016) 181–188, https://doi.org/10.1016/j.nme.2016.06.003.

[17] P. Lied, C. Bonnekoh, W. Pantleon, M. Stricker, A. Hoffmann, J. Reiser, Comparison of K-doped and pure cold-rolled tungsten sheets: As-rolled condition and recrystallization behaviour after isochronal annealing at different temperatures, Int. J. Refract. Met. Hard Mater. 85 (2019) 105047, https://doi.org/10.1016/j.ijrmhm.2019.105047.

[18] J. Reiser, C. Bonnekoh, T. Karcher, W. Pfleging, D. Weygand, A. Hoffmann, Recrystallisation towards a single texture component in heavily cold rolled tungsten (W) sheets and its impact on micromechanics, Int. J. Refract. Met. Hard Mater. 86 (2020) 105084, https://doi.org/10.1016/j.ijrmhm.2019.105084.

[19] C. Bonnekoh, P. Lied, W. Pantleon, T. Karcher, H. Leiste, A. Hoffmann, J. Reiser, M. Rieth, The brittle-to-ductile transition in cold-rolled tungsten sheets: On the loss of room-temperature ductility after annealing and the phenomenon of 45° embrittlement, Int. J. Refract. Met. Hard Mater. 93 (2020) 105347, https://doi.org/10.1016/j.ijrmhm.2020.105347.

[20] L. Tanure, A. Bakaeva, A. Dubinko, D. Terentyev, K. Verbeken, Effect of annealing on microstructure, texture and hardness of ITER-specification tungsten analyzed by EBSD, vickers micro-hardness and nano-indentation techniques, J. Nucl. Mater. 524 (2019) 191–199, https://doi.org/10.1016/j.jnucmat.2019.07.005.

[21] S. Nogami, A. Hasegawa, M. Fukuda, M. Rieth, J. Reiser, G. Pintsuk, Mechanical properties of tungsten: Recent research on modified tungsten materials in Japan, J. Nucl. Mater. 543 (2021) 152506, https://doi.org/10.1016/j.jnucmat.2020.152506.

[22] M. Mabuchi, K. Okamoto, N. Saito, M. Nakanishi, Y. Yamada, T. Asahina, T. Igarashi, Tensile properties at elevated temperature of W-1%La2O3, Mater. Sci. Eng. A 214 (1-2) (1996) 174–176, https://doi.org/10.1016/0921-5093(96)10377-4.

[23] M. Mabuchi, K. Okamoto, N. Saito, T. Asahina, T. Igarashi, Deformation behavior and strengthening mechanisms at intermediate temperatures in W-La2O3, Mater. Sci. Eng. A 237 (2) (1997) 241–249, https://doi.org/10.1016/S0921-5093(97)00420-6.

[24] T. Palacios, J. Reiser, J. Hoffmann, M. Rieth, A. Hoffmann, J.Y. Pastor, Microstructural and mechanical characterization of annealed tungsten (W) and potassium-doped tungsten foils, Int. J. Refract. Met. Hard Mater. 48 (2015) 145–149, https://doi.org/10.1016/j.ijrmhm.2014.09.005.

[25] J.W. Coenen, S. Antusch, M. Aumann, W. Biel, J. Du, J. Engels, S. Heuer, A. Houben, T. Hoeschen, B. Jasper, F. Koch, J. Linke, A. Litnovsky, Y. Mao, R. Neu, G. Pintsuk, J. Riesch, M. Rasiński, J. Reiser, M. Rieth, A. Terra, B. Unterberg, T. Weber, T. Wegener, J.-H. You, C. Linsmeier, Materials for DEMO and reactor applications - boundary conditions and new concepts, Phys. Scr. T167 (2016) 014022, https://doi.org/10.1088/0031-8949/2016/T167/014002.

[26] J. Reiser, M. Rieth, A. Möslang, B. Dafferner, J. Hoffmann, T. Mrotzek, A. Hoffmann, D.E.J. Armstrong, X. Yi, Tungsten foil laminate for structural divertor applications – Joining of tungsten foils, J. Nucl. Mater. 436 (1-3) (2013) 47–55, https://doi.org/10.1016/j.jnucmat.2013.01.295.

[27] J. Reiser, L.M. Garrison, H. Greuner, J. Hoffmann, T. Weingärtner, U. Jäntsch, M. Klimenkov, P. Franke, S. Bonk, C. Bonnekoh, S. Sickinger, S. Baumgärtner, D. Bolich, M. Hoffmann, R. Ziegler, J. Konrad, J. Hohe, A. Hoffmann, T. Mrotzek, M. Seiss, M. Rieth, A. Möslang, Ductilisation of tungsten (W): Tungsten laminated composites, Int. J. Refract. Met. Hard Mater. 69 (2017) 66–109, https://doi.org/10.1016/j.ijrmhm.2017.07.013.

[28] R.G. Abernethy, Predicting the performance of tungsten in a fusion environment: a literature review, Mater. Sci. Technol. 33 (4) (2017) 388–399, https://doi.org/10.1080/02670836.2016.1185260.

[29] T. Tanno, A. Hasegawa, J.-C. He, M. Fujiwara, S. Nogami, M. Satou, T. Shishido, K. Abe, Effects of Transmutation Elements on Neutron Irradiation Hardening of Tungsten, Mater. Trans. 48 (9) (2007) 2399–2402, https://doi.org/10.2320/matertrans.MAW200722.

[30] M. Fukuda, K. Yabuuchi, S. Nogami, A. Hasegawa, T. Tanaka, Microstructural development of tungsten and tungsten-rhenium alloys due to neutron irradiation in HFIR, J. Nucl. Mater. 455 (1-3) (2014) 460–463, https://doi.org/10.1016/j.jnucmat.2014.08.002.

[31] D. Stork, R. Heidinger, T. Muroga, S.J. Zinkle, A. Moeslang, M. Porton, J. Boutard, S. Gonzalez, A. Ibarra, Towards a programme of testing and qualification for structural and plasma-facing materials in "fusion neutron" environments, Nucl. Fusion 57 (2017) 092013, https://doi.org/10.1088/1741-4326/aa60af.

[32] S. Sato, Y. Verzilov, K. Ochiai, M. Nakao, M. Wada, N. Kubota, K. Kondo, M. Yamauchi, T. Nishitani, Progress in the blanket neutronics experiments at JAERI/FNS, Fusion Eng. Des. 81 (8-14) (2006) 1183–1193, https://doi.org/10.1016/j.fusengdes.2005.09.078.

[33] M. Martone, M. Angelone, M. Pillon, The 14 MeV Frascati neutron generator, J. Nucl. Mater. 212–215 (1994) 1661–1664, https://doi.org/10.1016/0022-3115(94)91109-6.

[34] S.J. Zinkle, M. Victoria, K. Abe, Scientific and engineering advances from fusion materials R&D, J. Nucl. Mater. 307–311 (2002) 31–42, https://doi.org/10.1016/S0022-3115(02)01088-7.
[35] K. Ehrlich, A. Möslang, IFMIF – An international fusion materials irradiation facility, Nucl. Instrum. Methods Phys. Res. Sect. B Beam Interact. Mater. Atoms. 139 (1998) 72–81. 10.1016/S0168-583X(97)01006-9.
[36] H. Dzitko, P. Cara, Y. Carin, S. Chel, A. Facco, D. Gex, K. Hasegawa, A. Kasugai, K. Kondo, V. Massaut, J. Molla, G. Phillips, A. Pisent, K. Sakamoto, M. Sugimoto, Status and future developments of the Linear IFMIF Prototype Accelerator (LIPAc), Fusion Eng. Des. 168 (2021) 112621, https://doi.org/10.1016/j.fusengdes.2021.112621.
[37] M. Cappelli, A. Bagnasco, J. Diaz, J. Sousa, F. Ambi, A. Campedrer, D. Liuzza, B. Carvalho, A. Ibarra, Status of the engineering design of the IFMIF-DONES Central Instrumentation and Control Systems, Fusion Eng. Des. 170 (2021) 112674, https://doi.org/10.1016/j.fusengdes.2021.112674.
[38] D. Bernardi, F. Arbeiter, M. Cappelli, U. Fischer, A. García, R. Heidinger, W. Krolas, F. Martín-Fuertes, G. Miccichè, A. Muñoz, F.S. Nitti, M. Pérez, T. Pinna, K. Tian, A. Ibarra, Towards the EU fusion-oriented neutron source: The preliminary engineering design of IFMIF-DONES, Fusion Eng. Des. 146 (2019) 261–268, https://doi.org/10.1016/j.fusengdes.2018.12.042.
[39] A. Ibarra, F. Arbeiter, D. Bernardi, M. Cappelli, A. García, R. Heidinger, W. Krolas, U. Fischer, F. Martin-Fuertes, G. Micciché, A. Muñoz, F.S. Nitti, M. Pérez, T. Pinna, K. Tian, The IFMIF-DONES project: preliminary engineering design, Nucl. Fusion. 58 (2018) 105002, https://doi.org/10.1088/1741-4326/aad91f.
[40] T. Suzudo, M. Yamaguchi, A. Hasegawa, Stability and mobility of rhenium and osmium in tungsten: first principles study, Model. Simul. Mater. Sci. Eng. 22 (7) (2014) 075006, https://doi.org/10.1088/0965-0393/22/7/075006.
[41] L.M. Garrison, Y. Katoh, L.L. Snead, T.S. Byun, J. Reiser, M. Rieth, Irradiation effects in tungsten-copper laminate composite, J. Nucl. Mater. 481 (2016) 134–146, https://doi.org/10.1016/j.jnucmat.2016.09.020.
[42] D. Terentyev, M. Rieth, G. Pintsuk, J. Riesch, A. von Müller, S. Antusch, K. Mergia, E. Gaganidze, H.-C. Schneider, M. Wirtz, S. Nogami, J. Coenen, J.H. You, A. Zinovev, W. Van Renterghem, Recent progress in the assessment of irradiation effects for in-vessel fusion materials: tungsten and copper alloys, Nucl. Fusion. 62 (2) (2022) 026045, https://doi.org/10.1088/1741-4326/ac4062.
[43] D. Jiang, J. Long, M. Cai, Y. Lin, P. Fan, H. Zhang, M. Zhong, Femtosecond laser fabricated micro/nano interface structures toward enhanced bonding strength and heat transfer capability of W/Cu joining, Mater. Des. 114 (2017) 185–193, https://doi.org/10.1016/j.matdes.2016.11.094.
[44] T. Zeng, F. Li, Y. Huang, Construction of an n-Body Potential for Revealing the Atomic Mechanism for Direct Alloying of Immiscible Tungsten and Copper, Mater. (Basel) 14 (2021) 5988, https://doi.org/10.3390/ma14205988.
[45] L.K. Keys, J.P. Smith, J. Moteff, High-temperature recovery of tungsten after neutron irradiation, Phys. Rev. 176 (3) (1968) 851–856, https://doi.org/10.1103/PhysRev.176.851.
[46] P.R. Okamoto, L.E. Rehn, Radiation-induced segregation in binary and ternary alloys, J. Nucl. Mater. 83 (1) (1979) 2–23, https://doi.org/10.1016/0022-3115(79)90587-7.
[47] D. Terentyev, M. Klimenkov, L. Malerba, Confinement of motion of interstitial clusters and dislocation loops in BCC Fe-Cr alloys, J. Nucl. Mater. 393 (1) (2009) 30–35, https://doi.org/10.1016/j.jnucmat.2009.05.002.
[48] D. Terentyev, A. Bakaev, Radiation-induced strengthening and absorption of dislocation loops in ferritic Fe–Cr alloys: the role of Cr segregation, J. Phys. Condens. Matter. 25 (26) (2013) 265702, https://doi.org/10.1088/0953-8984/25/26/265702.
[49] G.S. Was, Fundamentals of radiation materials science: Metals and alloys, Springer-Verlag, Berlin Heidelberg, 2007.
[50] R.K. Williams, F.W. Wiffen, J. Bentley, J.O. Stiegler, Irradiation induced precipitation in tungsten based, W-Re alloys, Metall. Trans. A. 14 (3) (1983) 655–666, https://doi.org/10.1007/BF02643781.
[51] R. Herschitz, D.N. Seidman, An atomic resolution study of homogeneous radiation-induced precipitation in a neutron irradiated W-10at.% Re alloy, Acta Metall. 32 (8) (1984) 1141–1154, https://doi.org/10.1016/0001-6160(84)90121-4.
[52] R. Herschitz, D.N. Seidman, An atomic resolution study of radiation-induced precipitation and solute segregation effects in a neutron-irradiated W-25 at.% Re alloy, Acta Metall. 32 (8) (1984) 1155–1171, https://doi.org/10.1016/0001-6160(84)90122-6.
[53] Carsten Bonnekoh, Philipp Lied, Stefan Zaefferer, Ute Jäntsch, Andreas Hoffmann, Jens Reiser, Michael Rieth, The brittle-to-ductile transition in cold-rolled tungsten sheets: Contributions of grain and subgrain boundaries to the enhanced ductility after pre-deformation, Nucl. Mater. Energy. 25 (2020) 100769, https://doi.org/10.1016/j.nme.2020.100769.
[54] T. Hirai, S. Panayotis, V.R. Barabash, C. Amzallag, F. Escourbiac, A. Durocher, M. Merola, J. Linke, T. Loewenhoff, G. Pintsuk, M. Wirtz, I. Uytdenhouwen, Use of tungsten material for the ITER divertor, Nucl. Mater. Energy 9 (2016) 616–622, https://doi.org/10.1016/j.nme.2016.07.003.
[55] M. Wirtz, J. Linke, T. Loewenhoff, G. Pintsuk, I. Uytdenhouwen, Thermal shock tests to qualify different tungsten grades as plasma facing material, Phys. Scr. T167 (2016) 014015, https://doi.org/10.1088/0031-8949/T167/1/014015.
[56] A. Dubinko, D. Terentyev, A. Bakaeva, K. Verbeken, M. Wirtz, M. Hernández-Mayoral, Evolution of plastic deformation in heavily deformed and recrystallized tungsten of ITER specification studied by TEM, Int. J. Refract. Met. Hard Mater. 66 (2017) 105–115, https://doi.org/10.1016/j.ijrmhm.2017.03.004.
[57] D. Terentyev, C.-C. Chang, C. Yin, A. Zinovev, X.-F. He, Neutron irradiation effects on mechanical properties of ITER specification tungsten, Tungsten (2021), https://doi.org/10.1007/s42864-021-00105-6.
[58] A. Zinovev, L. Delannay, D. Terentyev, Plastic deformation of ITER specification tungsten: Temperature and strain rate dependent constitutive law deduced by inverse finite element analysis, Int. J. Refract. Met. Hard Mater. 96 (2021), 105481, https://doi.org/10.1016/j.ijrmhm.2021.105481.
[59] C. Yin, D. Terentyev, T. Pardoen, R.H. Petrov, Z. Tong, Ductile to brittle transition in ITER specification tungsten assessed by combined fracture toughness and bending tests analysis, Mater. Sci. Eng. A 750 (2019) 20–30, https://doi.org/10.1016/j.msea.2019.02.028.
[60] L.R. Greenwood, F.A. Garner, Transmutation of Mo, Re, W, Hf, and V in various irradiation test facilities and STARFIRE, J. Nucl. Mater. 212–215 (1994) 635–639, https://doi.org/10.1016/0022-3115(94)90136-8.
[61] A General Monte Carlo N-Particle (MCNP) Transport Code, (n.d.). https://mcnp.lanl.gov/.
[62] S.L. Dudarev, DPA definition and estimates, 2015. https://www-amdis.iaea.org/CRP/IrradiatedTungsten/RCM2/RCM2Presentation-DudarevDPA-2015-09-10.pdf.
[63] C. Yin, D. Terentyev, T. Pardoen, A. Bakaeva, R.H. Petrov, S. Antusch, M. Rieth, M. Vilémová, J. Matějíček, T. Zhang, Tensile properties of baseline and advanced tungsten grades for fusion applications, Int. J. Refract. Met. Hard Mater. 75 (2018) 153–162, https://doi.org/10.1016/j.ijrmhm.2018.04.003.
[64] H.B. Motra, J. Hildebrand, A. Dimmig-Osburg, Assessment of strain measurement techniques to characterise mechanical properties of structural steel, Eng. Sci. Technol. Int. J. 17 (4) (2014) 260–269, https://doi.org/10.1016/j.jestch.2014.07.006.
[65] G. Kresse, J. Hafner, Ab initio molecular dynamics for liquid metals, Phys. Rev. B - Condens. Matter Mater. Phys. 47 (1) (1993) 558–561, https://doi.org/10.1103/PhysRevB.47.558.
[66] G. Kresse, J. Furthmüller, Efficient iterative schemes for ab initio total-energy calculations using a plane-wave basis set, Phys. Rev. B - Condens. Matter Mater. Phys. 54 (16) (1996) 11169–11186, https://doi.org/10.1103/PhysRevB.54.11169.
[67] P.E. Blöchl, Projector augmented-wave method, Phys. Rev. B - Condens. Matter Mater. Phys. 50 (24) (1994) 17953–17979, https://doi.org/10.1103/PhysRevB.50.17953.
[68] G. Kresse, D. Joubert, From ultrasoft pseudopotentials to the projector augmented-wave method, Phys. Rev. B - Condens. Matter Mater. Phys. 59 (3) (1999) 1758–1775, https://doi.org/10.1103/PhysRevB.59.1758.
[69] John P. Perdew, Kieron Burke, Matthias Ernzerhof, Generalized Gradient Approximation Made Simple, Phys. Rev. Lett. 77 (18) (1996) 3865–3868, https://doi.org/10.1103/PhysRevLett.77.3865.
[70] A. Bakaev, A. Zinovev, D. Terentyev, G. Bonny, C. Yin, N. Castin, Y.A. Mastrikov, E. E. Zhurkin, Interaction of carbon with microstructural defects in a W-Re matrix: An ab initio assessment, J. Appl. Phys. 126 (2019) 075110, https://doi.org/10.1063/1.5094441.
[71] A. Bakaev, D. Terentyev, X. He, D. Van Neck, Synergetic effects of Mn and Si in the interaction with point defects in bcc Fe, J. Nucl. Mater. 455 (1-3) (2014) 5–9, https://doi.org/10.1016/j.jnucmat.2014.02.033.